ROBERT N. McDONOUGH, BARRY E. RAFF, and JOYCE L. KERR

IMAGE FORMATION FROM SPACEBORNE SYNTHETIC APERTURE RADAR SIGNALS

The transformation of synthetic aperture radar (SAR) phase history data into images is a significant signal processing problem. APL is one of a relatively few facilities that can digitally process satellite SAR data. Development of the processor requires the availability of a high-speed computer system and the use of complex algorithms for efficient operation. The algorithms, in essence, perform a two-dimensional convolution of the radar returns with a nonstationary matched filter. The resultant image quality depends on the accuracy maintained in reconstructing the complete radar signal phase history and in compensating for such effects as beam squint, earth rotation, and range cell migration. This article describes in some detail the APL processing algorithms and implementation techniques. Examples are presented to show that the processor attains theoretical resolution limits.

INTRODUCTION

On June 28, 1978, NASA launched Seasat, the first earth-orbiting satellite specifically designed for remote sensing of the oceans. Seasat carried instruments to perform five integrated experiments intended to characterize the oceanographic environment (surface winds, wave fields, cloud cover, and water features).[1] One of the instruments[2] was unprecedented: a synthetic aperture radar (SAR) that produced a wealth of data that is still being processed and analyzed. The variety and detail of features in Seasat imagery of both land and ocean were unexpected, spawning new theories that are still being constructed, debated, and tested.[3] Similar instruments, Shuttle Imaging Radars (SIR), were launched in 1981 (SIR-A) and 1984 (SIR-B), and more are planned for launches into the 1990s by NASA, the European Space Agency, Canada, and Japan.

SAR images are of intense interest in many disciplines (geology, oceanography, hydrology, archaeology, etc.). However, significant signal processing is required to produce intelligible imagery from raw radar signals. This article will describe the computer algorithms that were developed and implemented at APL to produce SAR images from a variety of instruments carried on both spacecraft and aircraft platforms. The APL processor provides a versatile test bed for experimentation with processing and information-extraction algorithms to determine target attributes from radar data.

BACKGROUND

The processing of raw data to form a SAR image can be accomplished using optical equipment or a digital computer. In the former case, the radar output signal is recorded as intensity modulation on photographic film. This "signal" film is then illuminated by a spatially coherent light source, and the transmitted light is focused using conical and spherical lenses that provide an appropriate phase shift for each point of the radar signal history. The specially designed analog equipment can operate essentially in real time, producing images in hard or soft format. Optical SAR processing was used in the earliest SAR systems and is still commonly employed for "quick-look" surveillance and cataloging.

Digital processing, on the other hand, presents an intensive computational challenge. Real-time processing of SAR signals from space platforms is regarded as feasible, but to date it is an unrealized goal. Nevertheless, because of its great flexibility, accuracy, and stability, digital SAR processing is currently of great interest.

In 1981, APL acquired a then-unique computer resource, one of the first Floating Point Systems FPS-164 attached array processors. Linked with a VAX-11/780 mainframe (Fig. 1), the system provides pipelined computational speeds of 11 megaflops, a large array processor memory of 1.7 megawords (64 bits), and a large library of Fortran-callable subroutines. Due in part to the availability of this powerful computing resource, APL was asked by the Defense Advanced Research Projects Agency to develop a digital algorithm for SAR image processing of raw radar signals. After reviewing the information generally available and after investigating the possibility of acquiring a commercially available code, it was decided to design and implement a custom algorithm for our specific resources and requirements.

The processor was designed to be highly modular (allowing easy adaptation to different signal sources) and to make extensive use of the FPS-164 mathematics library routines optimized for the array processor. The Seasat SAR was selected as the first signal source because the data were readily available and the processing problem was general and demanding. To date, the basic processor has been successfully employed

Figure 1—VAX-11/780 computer (right) and FPS-164 attached processor (left).

with data from Seasat, SIR-A, SIR-B, and the Canadian CV-580 aircraft.

SAR SIMPLIFIED

The key elements of SAR can be understood in the following simple overview. Suppose a radar is carried on a vehicle at an altitude, h, and views the earth as shown in Fig. 2. The radar looks down and to the side and has an along-track field of view determined by the antenna beamwidth, θ_B. For large time-bandwidth systems, the range resolution, δr, is $\delta r = c/2B_r$, where c is the speed of light and B_r is the bandwidth of the system pulse. Thus, δr can be made quite small (on the order of a few meters) by using a large bandwidth. On the other hand, the along-track resolution, δx, for a real aperture radar is of the order of $\delta x = h\lambda/L$, where λ is the radar wavelength and L is the physical antenna aperture. For reasonable values of $h = 800$ kilometers and $\lambda = 0.235$ meter (the Seasat values), attaining a δx value of even 1 kilometer requires an antenna length, L, of 188 meters, which is inconveniently large.

However, SAR systems resolve this difficulty. The attainable resolution in along-track time, $\delta\tau$, is $\delta\tau = 1/B_D$, where B_D is the Doppler spectrum bandwidth, a result that will be derived below. The Doppler spectrum is caused directly by viewing a target from different aspect angles as the vehicle moves. In order to realize the SAR effect, this Doppler spectrum must be produced, which requires two crucial elements: (1) the radar must be side-looking (head-on aspect produces an along-track measurement that is redundant with the range measurement), and (2) the radar must be time-coherent from pulse to pulse. Then the radar return from a point at slant range, r, from the radar will have an exploitable phase, $\phi(\tau)$, of $\phi(\tau) = 4\pi r(\tau)/\lambda$, where τ is the time along the vehicle track. The Doppler frequency, f_D, is $f_D = -\dot{\phi}(\tau)/2\pi = -2\dot{r}(\tau)/\lambda \approx -2V\theta/\lambda$ for small values of θ, where V is the vehicle speed and θ is the angle of the ray from the radar to the ground point in question, measured relative to the radar beam center. Since the field of view is limited by the real antenna length, $|\theta| < \theta_B/2 = \lambda/2L$, then $B_D = 2V/L$, and $\delta x = V\,\delta\tau = L/2$. Thus, for example, a SAR system with a real antenna length of 11 meters (Seasat) provides a system resolution of 5.5 meters. In contrast, the same system using only the real aperture would have a system resolution of $h\lambda/L$, or approximately 17 kilometers. The advantage of SAR is obvious.

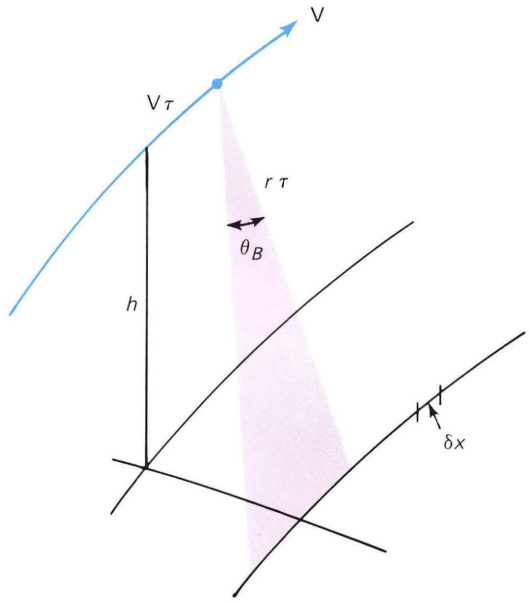

Figure 2—Simplified geometry of radar vehicle in flight over a target surface.

THE SAR SIGNAL

In order to understand in some detail the SAR processing algorithm, it is necessary to understand the nature of the raw radar signal. Consider the situation shown in Fig. 3. Here a satellite at altitude, h, flies in a locally circular orbit over a nominally spherical earth. Let the ground coordinate system be as shown, where r_0 is the range between some arbitrary fixed earth point and the satellite at the point of closest approach, and τ_0 is the time at which the satellite passes at closest approach.

The radar emits pulses that travel to the earth point (τ_0, r_0) and are reflected back. The vehicle speed is much less than the speed of light, so the radar can be considered to be at a fixed position during the time that the pulse interacts with the earth point (this is the "start-stop" approximation). Now suppose that the radar emits a pulse waveform in time, t, with a complex envelope, $a(t,\tau)$, where the time, τ, defines the satellite location (because its ephemeris is known), and let the origin of t be taken at, say, the time of transmission of the mid-point of the pulse. Consider only one reflector at the location (τ_0,r_0) with complex reflectivity, $\sigma(\tau_0,r_0)$. Then the received signal is given by

$$g(t,\tau\,|\tau_0,r_0) = \sigma(\tau_0,r_0)\; a[t - 2r(\tau)/c,\ \tau] \times \exp\{-j\omega_0[t - 2r(\tau)/c]\}\ ,$$

where ω_0 is the carrier radian frequency of the radar pulse and $r(\tau)$ is the slant range from the radar position at the time τ to the target at the position (τ_0,r_0).

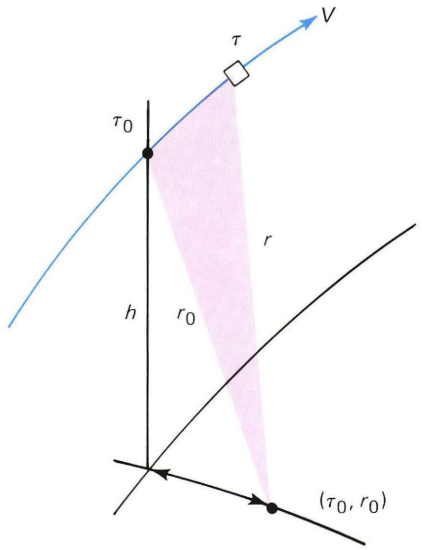

Figure 3—Geometry of radar vehicle in flight past a hypothetical isolated point target.

Here the "start-stop" approximation is used, in that the round-trip travel distance is just $2r$, independent of time within the pulse. The radar receives the scattered pulse some tens of meters (40 meters for Seasat) farther along the track than where it transmitted the pulse. This introduces a bias of tens of meters in along-track location of the final image, an effect that we shall ignore.

The radar system is nominally linear, so that with a distributed reflectivity map, $\sigma(\tau_0,r_0)$, the received signal, $g(t,\tau)$, is found from

$$g(t,\tau) = \int_{T_0}\int_{R_0} \sigma(\tau_0,r_0)\, a[t - 2r(\tau)/c,\ \tau] \times \exp\{-j\omega_0[t - 2r(\tau)/c]\}\ dr_0 d\tau_0 ,$$

$$t \in T,\ \tau \in \mathrm{T} ,$$

where (T_0,R_0) is the region of earth surface illuminated by the radar beam with the satellite at the position corresponding to the time, τ, and (T,T) is the domain over which signals are collected. Thus, the raw SAR signal is modeled as a two-dimensional convolution of the complex reflectivity map, $\sigma(\tau_0,r_0)$, with an impulse response (or Green's function) of

$$h(t,\tau\,|\tau_0,r_0) = a[t - 2r(\tau)/c,\ \tau] \times \exp\{-j\omega_0[t - 2r(\tau)/c]\} .$$

THE IMAGE-FORMATION ALGORITHM

It is desired to produce an image of $|\sigma(\tau_0,r_0)|$, or of its square, the intensity map. This requires implementing the inverse Green's function, h^{-1}, and using it to process the radar data:

$$\sigma(\tau_0,\mathrm{r}_0) = \int_T \int_{\mathrm{T}} g(t,\tau)\ h^{-1}(\tau_0,r_0\,|t,\tau)\ dt\ d\tau ,$$

where, by definition,

$$\int_T \int_{\mathrm{T}} h^{-1}(\tau_0,r_0\,|t,\tau)\ h(t,\tau\,|\tau_0{}',r_0{}')\ dt\ d\tau = \delta(\tau_0 - \tau_0{}',\ r_0 - r_0{}') ,$$

which is the Dirac delta function.

It is important to note that a description of how to treat the raw data, $h(t,\tau\,|\tau_0',r_0')$, from an isolated point target, $\sigma(\tau_0,r_0) = \delta(\tau_0 - \tau_0',\ r_0 - r_0')$, to produce the image of that point target is sufficient to describe how to implement h^{-1} as applied to all the radar signals, and hence the whole SAR processing algorithm. Note particularly that this argument assumes only linearity of the radar system, not stationarity (i.e., $h(t,\tau\,|\tau_0,r_0) \neq h(t - 2r_0/c,\ \tau - \tau_0)$. This nonstationarity of the "filter," and thereby its inverse, is responsible for a considerable amount of the complexity of the processor algorithm.

Consider, then, the response of the radar to a single point target. This is

$$g(t,\tau) = a[t - 2r(\tau)/c,\ \tau] \exp\{-j\omega_0[t - 2r(\tau)/c]\} .$$

To achieve fine range resolution, the radar transmits a pulse $s(t)$, with a large time-bandwidth product, typically a linear-frequency modulated (chirped) sinusoid:

$$s(t) = \cos 2\pi(f_0 t + \tfrac{1}{2} K_r t^2) , \qquad |t| \leq \Delta t/2 ,$$

where f_0 is the carrier frequency of the pulse, K_r is the frequency sweep rate, and where $t = 0$ for the pulse, k, is taken at the along-track time, τ_k, of the pulse mid-point. The rate of change of phase is $f_0 + K_r t$, and the nominal bandwidth is $B_r = K_r(\Delta t)$ centered at f_0. The received pulse is

$$g(t) = \cos\{2\pi f_0[t - 2r(\tau)/c] + \pi K_r[t - 2r(\tau)/c]^2\} ,$$

$$|t - 2r(\tau)/c| \leq \Delta t/2 ,$$

and has the same amplitude spectrum as the transmitted pulse. For ease in processing, this analog signal is down-converted to an intermediate frequency, f_1, much less than f_0, with $f_1 \geq B_r/2$. (For Seasat, $f_0 =$ 1275 megahertz, $f_1 =$ 11.38 megahertz (the "offset video frequency"), and $B_r =$ 19.0 megahertz.)

The down-converted received signal, described by

$$g'(t) = \cos\{2\pi[f_1 t - 2r(\tau)/\lambda] + \pi K_r[t - 2r(\tau)/c]^2\} ,$$

has a large time extent, Δt, and offers no useful target range resolution. However, when correlated[4] with

an appropriate down-converted replica, $s'(-t)$, (matched filtering), the resulting output is

$$s'(-t)*g'(t) \approx \frac{\Delta t}{2}\,\mathrm{Re}\left(\frac{\sin \pi B_r[t - 2r(\tau)/c]}{\pi B_r[t - 2r(\tau)/c]} \times \{\exp[-j4\pi r(\tau)/\lambda]\}[\exp(j2\pi f_1 t)]\right),$$

$$|t - 2r(\tau)/c| \leq \Delta t,$$

where $*$ represents the operation of convolution. The approximation is valid, provided that $B_r\Delta t = K_r\Delta t^2 \gg 1/\pi$, which is well satisfied in practice.

This basic result is a signal at the intermediate frequency with a complex envelope of nominal 3 decibel width, δt, of $\delta t = 1/B_r$ centered at $t_0 = 2r_0/c$. The envelope can be detected by left-shifting the signal by an amount equal to f_1. The position of the peak amplitude of the result then measures r_0 to a precision, δr, of $\delta r = c\delta t/2 = c/2B_r$ (the system slant-range resolution), while the value at that instant (dropping $\Delta t/2$) is the complex number $\exp(-j4\pi r_0/\lambda)$. Thus, this "range compression" or "de-chirp" operation has resulted in a filter output localized in range at the value, r_0, corresponding to our hypothesized isolated point target and has realized one dimension of the reassembly of the point-scattered radar return.

It is interesting to illustrate the process of range compression using a digitally processed Seasat scene near the Goldstone Tracking Station in the Mojave Desert of California (Fig. 4). The bright reflecting object evidenced by the cross to the left of the center of the figure is the SAR image of a 26 meter antenna. The antenna is so bright relative to its surroundings that it is easy to trace its signature throughout the various phases of the processor. The actual time waveform of the received reflection, $g(t)$, from the Goldstone antenna for one radar pulse is shown in Fig. 5a; the corresponding matched filter output is shown in Fig. 5b. It is important to remember that the compressed range data for each pulse are complex data of the form $\exp[-j4\pi r(\tau)/\lambda]$, and that, because the radar is coherent from pulse to pulse, these complex data exhibit the phase history of the target in terms of the slant range at each pulse. The next step is to compress the data along the flight ("azimuth") direction.

The azimuth compression procedure is entirely analogous to range compression. The range-compressed point target signal is $\exp[-j4\pi r(\tau)/\lambda]$, for values of r such that the target is in the real antenna beamwidth. Recalling that $r(\tau) = r(\tau\,|\tau_0, r_0)$ and designating τ_c as the time at which the target is at the center of the beam, then, to the second order of a Taylor expansion,

$$r(\tau) \approx r(\tau_c) + \dot{r}(\tau_c)(\tau - \tau_c) + \tfrac{1}{2}\ddot{r}(\tau_c)(\tau - \tau_c)^2,$$

where

$$|\tau - \tau_c| \lesssim r_c\theta_B/2V.$$

Figure 4—Seasat SAR image of a 50 × 70 kilometer region of the Mojave Desert showing Goldstone antenna (located at the cross to the left of center).

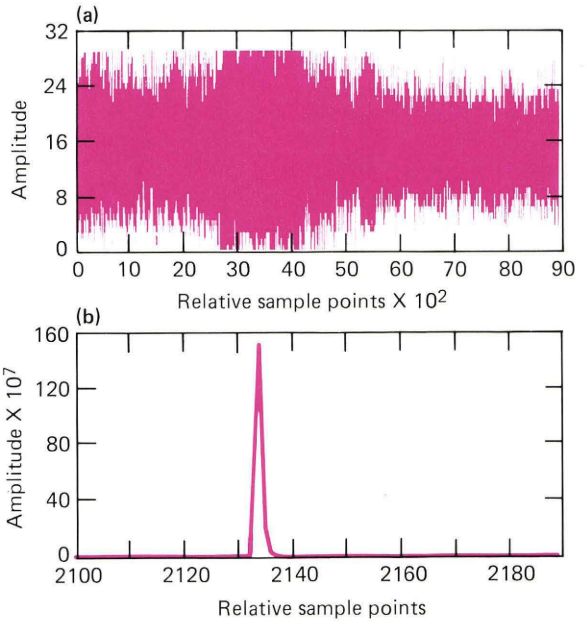

Figure 5—Range compression: (a) received reflection of Goldstone antenna; (b) Goldstone antenna target after range compression. The time history of the return from a single radar pulse is shown.

Defining the center frequency of the Doppler spectrum, f_{Dc}, the Doppler frequency sweep rate, K_{az}, and the time extent of the Doppler signal, $\Delta\tau$,

$$f_{Dc} = -2\dot{r}_c/\lambda,\ K_{az} = -2\ddot{r}_c/\lambda,\ \Delta\tau = r_c\theta_B/V,$$

and substituting the above expansion of $r(\tau)$, we obtain the complex output of the range compression filter,

$$g(\tau) = \begin{cases} \exp[-j4\pi r(\tau)/\lambda] = [\exp(-j4\pi r_c/\lambda)] \times \\ \{\exp[j2\pi f_{Dc}(\tau-\tau_c) + j\pi K_{az}(\tau-\tau_c)^2]\}, \\ \qquad |\tau-\tau_c| \lesssim \Delta\tau/2 \\ 0 \qquad \text{elsewhere}, \end{cases}$$

which is of the form treated earlier in the range dimension; i.e., we have a linearly frequency modulated waveform covering the band, B_D, where $B_D = |K_{az}\Delta\tau|$ centered at f_{Dc}, with the time and frequency being along-track flight time and Doppler frequency.

Thus, azimuth compression involves applying a matched filter with an impulse response of

$$h(\tau) = \exp[j2\pi(f_{Dc}\tau - \tfrac{1}{2} K_{az}\tau^2)] ,$$

$$|\tau| \leq \Delta\tau/2 ,$$

to the range-compressed signals. (The radar pulse repetition frequency (PRF) provides a natural sampling of the azimuth signal.) The matched filter output, assuming no aliasing (i.e., PRF $> B_D$) is the sequence of samples of

$$b(\tau) = g(\tau) * h(\tau)$$

$$\cong [\exp(j2\pi f_{Dc}\tau)]$$

$$\times \{\exp[-j2\pi(2r_c/\lambda + f_{Dc}\tau_c)]\}$$

$$\times \Delta\tau \left\{ \frac{\sin\pi B_D(\tau - \tau_c)}{\pi B_D(\tau - \tau_c)} \right\} ,$$

$$|\tau - \tau_c| \leq \Delta\tau/2 .$$

The amplitude of this signal peaks at $\tau = \tau_c$ and has a width, $\delta\tau$, of $\delta\tau = 1/B_D$, which is, thereby, the system along-track time resolution, where B_D, the system Doppler bandwidth, is $B_D = |K_{az}|(\Delta\tau)$. Again, the approximation is used that $B_D(\Delta\tau) \gg 1/\pi$. (For Seasat, $B_D(\Delta\tau) \approx (1300)(2.5) = 3250$.) The oscillatory factor at the frequency, f_{Dc}, is of no consequence if only $|b(\tau)|$ is of interest, as in reconstructing an intensity map. However, it can be removed by complex demodulation in the τ domain.

Four practical effects mar the conceptual simplicity of the azimuth matched filter and account for most of the difficulty in building a SAR processor. First, the collected data are range ordered, pulse-by-pulse, but the azimuth filter requires access to the data in opposite order, which necessitates a transposition ("corner turning") procedure. Second, the slant range of the point target can change significantly while the target is in view, and the data corresponding to a particular point target migrate through range cells on sequential radar pulses. This is the "range migration" problem and requires that data for each azimuth matched filter (one for each value of r_c of interest) be assembled from along a curved trajectory in the (r, τ)-indexed data matrix. This is accomplished by re-indexing and interpolating through the data matrix at various points. Third, the parameters f_{Dc} and K_{az} are not necessarily known a priori and must be estimated from the actual data using the "clutter-lock" and "autofocus" procedures. Finally, both f_{Dc} and K_{az} depend on r_c, so that the azimuth filter changes over the image, necessitating use of models for $f_{Dc}(r_c)$ and $K_{az}(r_c)$. These problems, together with details of the algorithm, are considered in the Specific Procedures section below.

One final operation is often performed, "multi-look processing." As with any phase-coherent imaging system, SAR is subject to "speckle noise," which appears as random light and dark patches caused by constructive and destructive interference from object facets having a physical extent on the order of a wavelength. This "noise" pattern depends on the viewing angle, since the pattern of small-scale reflectors depends on aspect. Multi-look processing exploits the fact that images from data taken at different aspect angles will have independent speckle patterns. The independent image intensity patterns are added incoherently, with the result that the sum has reduced speckle. The component multiple images are formed using data taken from separate intervals of the along-track radar beam, corresponding to sub-bands of the full available Doppler spectrum. Figure 6 shows the filters used for single-look and four-look processing, and Fig. 7 shows the four independent looks at the Goldstone target. The four looks are registered at along-track times separated by $(f_{Di} - f_{Dj})/K_{az}$ where f_{Di} and f_{Dj} are the center frequencies of sub-bands i and j, respectively. Figure 7 also shows the sum of the time-registered "looks."

PROCESSOR IMPLEMENTATION AND SPEED

The overall processor logic is shown in Fig. 8, and the arrangement of the data flow is shown in Fig. 9. The host VAX-11/780 reads an entire range line of data into the FPS-164 memory (13,680 samples for Seasat). Each range line is fast-compressed using a 16K

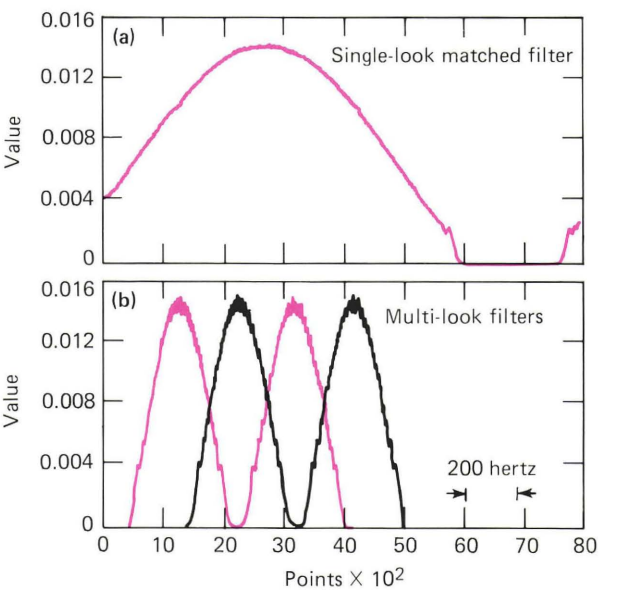

Figure 6—Amplitude spectrum of filters applied to Doppler spectrum of compressed range returns: (a) single-look processing; (b) four-look processing.

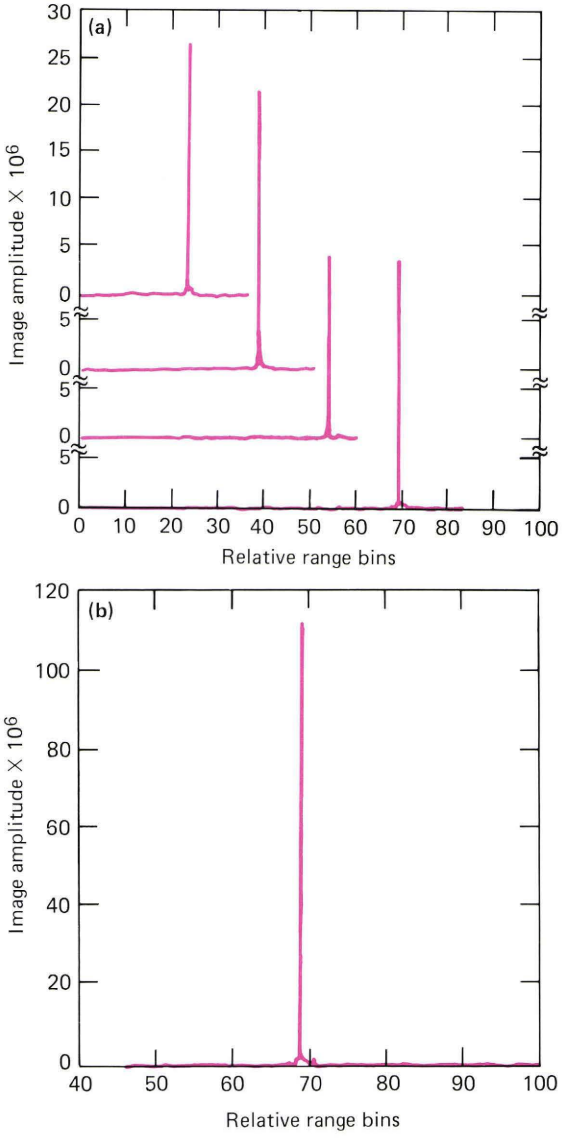

Figure 7—Outputs of azimuth compression filters for range bin at Goldstone target: (a) outputs of individual look filters in four-look processing; (b) result of time registration and summation of the four outputs.

fast Fourier transform and is interpolated to achieve correction of the dominant (linear) component of range migration. (Interpolation is done as part of range compression by using one of eight different matched filters that produce delays of 0 through 7/8 of a range sampling bin, together with sample re-indexing.) The process is repeated for 128 radar pulses, at which point the FPS memory is dumped to disk, with each 64 consecutive range bins being written to a different file. The entire process continues until 8192 pulses have been compressed. Each disk file then contains 8192 pulses of along-track data from 64 consecutive range bins. Each file is then read back into the FPS memory, one file at a time, and fast azimuth compression is carried out. No explicit corner-turning operation is needed.

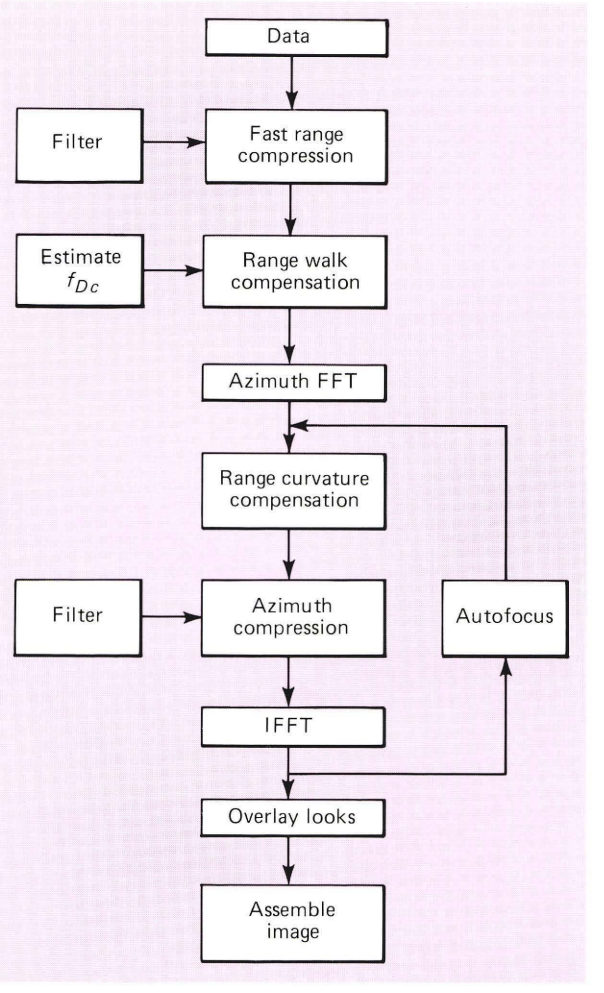

Figure 8—APL digital SAR processor, VAX-11/780, and FPS-164. FFT = fast Fourier transform; IFFT = inverse fast Fourier transform.

The algorithm for estimating f_{Dc} involves least-squares fitting of a model to representative Doppler spectra of raw uncompressed data. The particular model used depends on the specific radar system in question and on nominal platform parameters. In the autofocus procedure for determining K_{az}, two "looks" (sub-bands of the Doppler spectrum) are processed with a trial parameter value V^2 in the model $K_{az} = -2V^2/\lambda r_c$, and by correlation of the corresponding images a correction found for V^2 (the "sub-aperture correlation" method). (Determination of these two filter parameters is discussed in more detail in the Specific Procedures section.) The azimuth matched filter parameters are changed as r_c steps across the swath. For Seasat processing, the filter is updated each 64 range bins.

The quality of the resulting imagery can be assessed by examining the reconstruction of an isolated point target. The Goldstone antenna, while tutorially interesting, is unsuitable for this purpose because the receiver is saturated and hard-limiting on this very bright (and large) target (Fig. 5a). However, a constellation

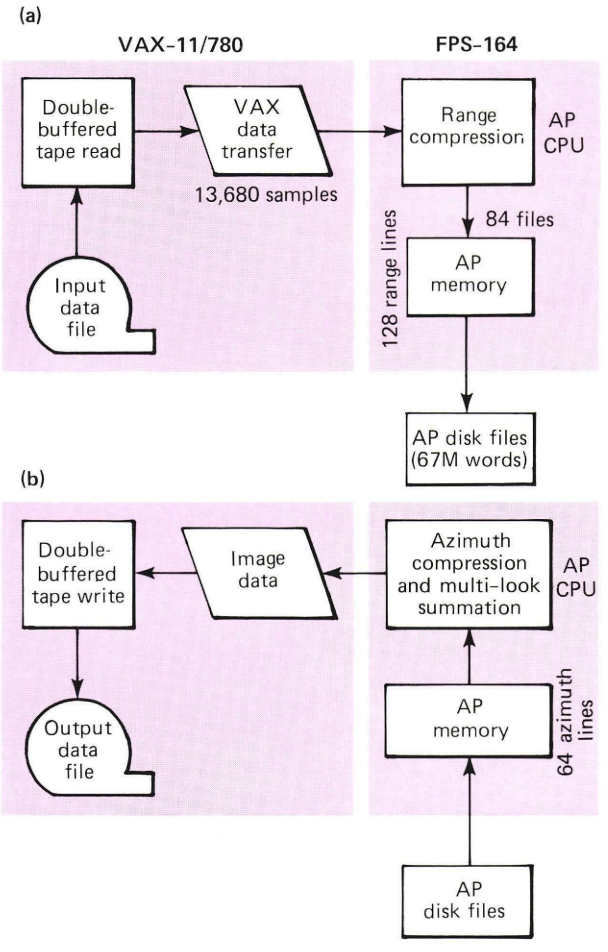

Figure 9—Data flow during (a) range compression and (b) azimuth compression. AP is the FPS-164 attached processor.

of corner reflectors deployed on the (dry) bed of Goldstone Lake near the antenna provides a more adequate test. Figure 10 shows the reconstructed image of one of these reflectors, together with the image intensity plots as taken along range and azimuth cuts through the central pixel. The resolution and sidelobe structure thereby displayed correspond closely to the theoretical values attainable for the Seasat system.

The time to produce a standard four-look 100 by 100 kilometer Seasat image is about 5 hours, using unoptimized Fortran code, which, although unoptimized, does take advantage of overlapped operations possible between the VAX-11/780 and the FPS-164. The current production processor operated by the Jet Propulsion Laboratory is optimized for speed and requires 2.7 hours, using three parallel AP120B processors driven by an SEL host computer. This is still about 580 times slower than real time. Processing in real time is currently feasible in dedicated hardware and is being developed at the Jet Propulsion Laboratory.

DATA PRODUCTS

The APL processor has been configured successively for Seasat, the SAR aboard the Canadian CV-580 aircraft, SIR-A, and SIR-B. Some images may be of interest.

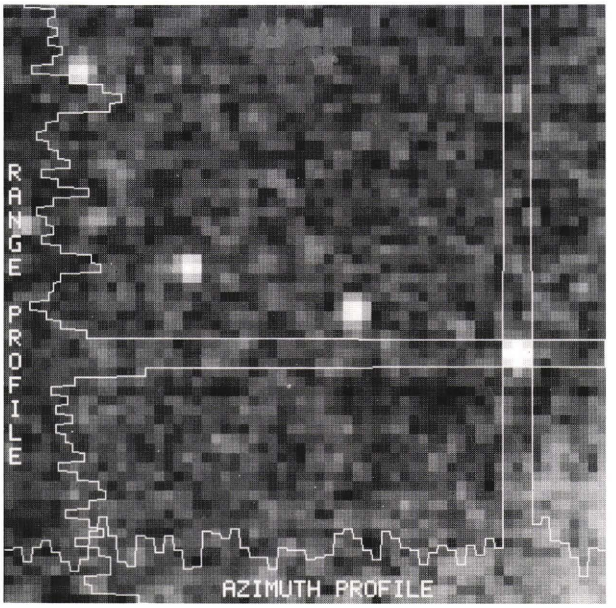

Figure 10—Point reflectors on Goldstone dry lake, showing attained resolution and sidelobe structure in range and azimuth.

In Fig. 11, we show an example of a Seasat scene with a subtle feature. The ship, observed in the English Channel on revolution 834, has a clearly evident Kelvin wake. More subtly, the transverse wake is visible as striations between the arms of the longitudinal Kelvin wake. The intensity has been plotted across the two sides of the Kelvin wake and the central turbulent wake, with averaging longitudinally between the limits indicated by the white cross lines. The small insets show the spatial autocorrelation function of the portion of the image hidden by the inset, which displays the processor impulse response function for this noise-like image.

Figure 12 shows an X-band scene from the system aboard the Canadian CV-580 aircraft, while Fig. 13 is an L-band scene from the same system flown over the Georgia Straits in British Columbia.

Figure 14 shows a land scene near Montreal, viewed by SIR-B from the space shuttle. An enlargement is shown in Fig. 15, together with an indication of the resolution obtained by noise correlation.

SPECIFIC PROCEDURES OF THE IMAGE FORMATION ALGORITHM

As we have discussed above, the SAR processing procedure amounts to two-dimensional matched filtering of the sampled radar data. Four practical problems arise in the azimuth (along-track) processing, which we will discuss here in some detail. These concern corner turning, range migration, modeling and estimation of the azimuth matched filter parameters, and changes in the azimuth filter as a function of range.

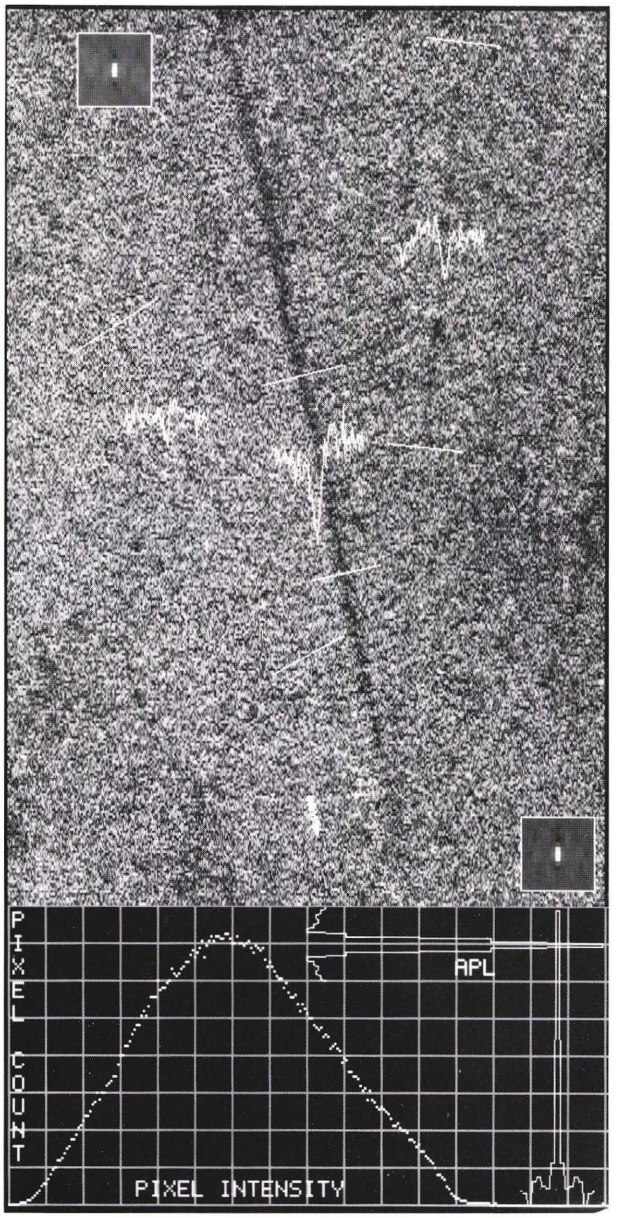

Figure 11—Seasat English Channel scene, showing transverse structure in ship wake and processor range and azimuth resolution and sidelobe structure as measured by noise autocorrelation.

The first problem, corner turning, arises because radar data are collected pulse by pulse and are stored, ordered first by range sample number and second by pulse number. This is what is needed for range compression, but after that operation the data must be reordered by pulse number first so that azimuth filtering can be done. As we discussed above, this reordering (corner turning) operation is carried out implicitly in our system by writing range-compressed data to disk files in an order that makes access for azimuth compression convenient.

Range migration occurs because data received from a point target (τ_0, r_0) at each pulse time, τ_k, are perceived at slant ranges $r_k(\tau_0, r_0)$ and not at the actual

Figure 12—Image of Ford Lake (Detroit), CV-580 radar.

range from track, r_0. Thus, the data from a point target lie on a curved trajectory described by

$$r(\tau) \approx r_c - (\lambda/2)[f_{Dc}\ (\tau - \tau_c) + \tfrac{1}{2}K_{az}(\tau - \tau_c)^2]\ ,$$

$$|\tau - \tau_c| \lesssim \Delta\tau/2\ ,$$

which can vary over many range sampling intervals during the period that the point (τ_0, r_0) is in view, as illustrated in Fig. 16. The matter is further complicated because the trajectory parameters f_{Dc} and K_{az} depend on r_c, the point-target slant range at beam center. The data corresponding to a particular pulse time, τ, are sampled and stored at memory locations corresponding to the complex range bin nearest the actual target slant range, r, for the particular time, τ. The point target data needed for azimuth compression would lie along the nearly parabolic trajectory in the memory matrix illustrated in Fig. 16 and are not readily available. Therefore, it is necessary to interpolate the stored data to locations along that parabola and then to store the results at locations in memory that can be accessed conveniently in columns. This process is accomplished in two steps—first, removal of most of the linear range walk, and second, removal of the quadratic curvature and residual linear walk.

First, a particular value of r_c is chosen, say the mid-swath value, r_c'. The corresponding Doppler center frequency, f_{Dc}', is found from the model developed below. As shown in Fig. 17, at the azimuth time, τ, the datum at the tail of each arrow along the corresponding range line is computed by interpolation and stored at the memory node at the arrow head. Thus, at the azimuth time, τ, the data are shifted left by an

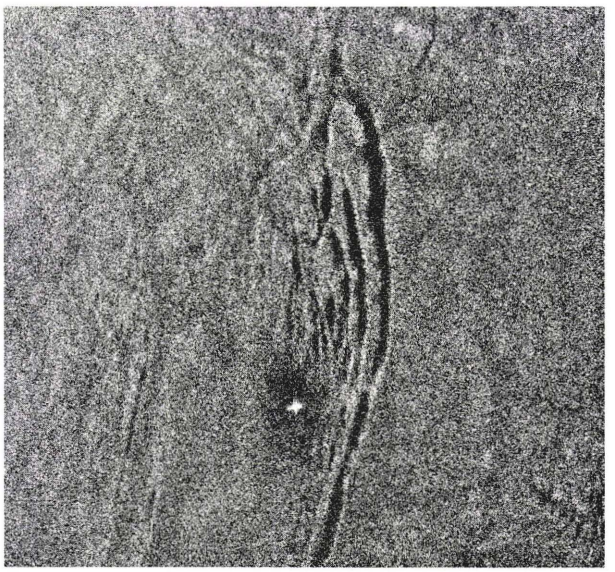

Figure 13—L-band image of internal waves in the Georgia Straits, CV-580 radar.

Figure 14—SIR-B image of Montreal.

Figure 15—Detail from Fig. 14, also showing processor resolution and sidelobe structure as measured by noise autocorrelation.

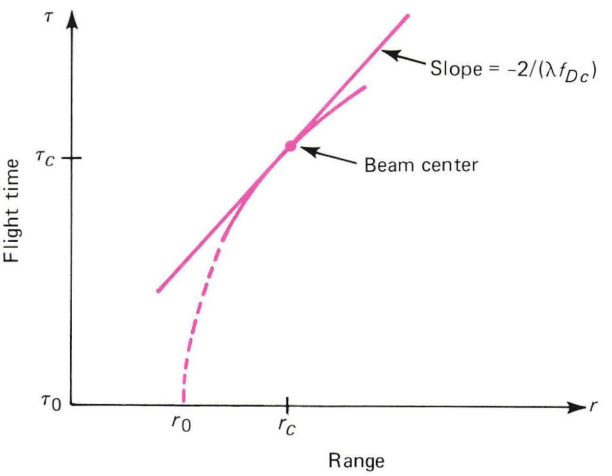

Figure 16—Range migration trajectory in the data matrix.

amount $\Delta r = -\lambda f'_{Dc}\,\tau/2$. Note that this does not remove the full amount of the linear range walk because a constant value f'_{Dc} is used for all values of r_c, not simply for r_c'. The residual will be removed later.

The values at the arrow tails in Fig. 17 are computed by interpolating the available complex data samples at the memory nodes. This could be done by interpolating the real and imaginary parts of the baseband complex range data, but it is possible to combine this step with the range compression filter, so that there is no separate interpolation step as such.

Consider a (real or complex) band-limited function $f(t)$, with a spectrum of $F(j\omega) = 0$, $|\omega| > \pi/\Delta t$, with Δt so defined. This function is sampled to produce the (possibly infinite) sequence $f_n = f(n\Delta t)$. Then[5] interpolated samples, $f[(n+\alpha)\Delta t,]$, of $f(t)$ are exactly

$$g_n = f(n\Delta t + \alpha\Delta t)$$

$$= \sum_{l=-\infty}^{\infty} f_l[\sin \pi(n+\alpha-l)]/\pi(n+\alpha-l) ,$$

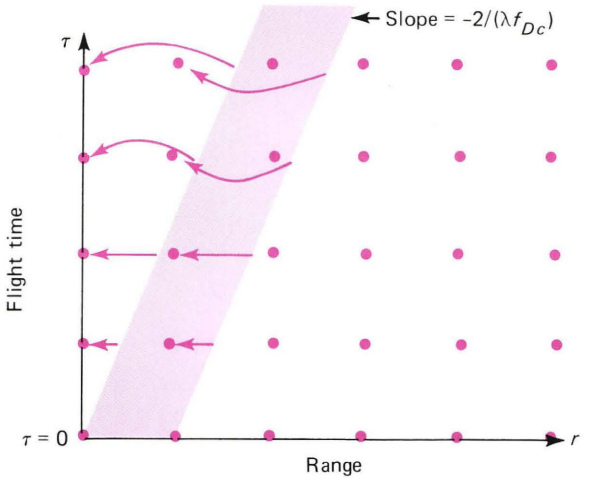

Figure 17—Nodes in the data matrix showing a scheme for nominal correction of the range migration effect.

i.e., the discrete convolution of the given samples, f_n, with the (infinite) sequence

$$h_n = \sin[\pi(n + \alpha)]/\pi(n + \alpha) .$$

This discrete convolution can be computed with a "fast" convolution, using the fast Fourier transform. Assume that $f_n \neq 0$ only over $0 \leq n < P$ and truncate the interpolator sequence as $h_n = 0$, $|n| > L$. Using a fast Fourier transform size $N \leq P + 2L$ avoids "wrap-around" effects that can otherwise arise from the circular nature of fast convolution. Assuming $|\alpha| < 1$ (which suffices), the sequence h_n, $n \leq L$, is replaced by the equivalent sequence (for fast convolution) $h_n' = h_n$, $n = 0, 1, \ldots, L$; $h_n' = 0$, $n = L + 1, \ldots, N-L-1$; $h_n' = h_{n-N}'$, $n = N - L, \ldots, N-1$. Then, except for truncation error,

$$g_n = \mathrm{IFFT}_N\{\mathrm{FFT}_N(f_n)\mathrm{FFT}_N(h_n')\} ,$$

$$n = 0, \ldots, P - 1 ,$$

where FFT and IFFT indicate the direct and inverse fast Fourier transform operations, respectively. The truncation error is negligible for moderately large values of L (e.g., $L > 50$), for which case the largest neglected value of h_n is 44 decibels below h_0.

Conceptually this interpolation operation is to be applied to the compressed baseband (complex) data. However, it could just as well be applied to the video offset carrier range data, which then allows the interpolation filter to be combined with the range compression filter. The fast Fourier transform of h_n' yields a baseband complex interpolator spectrum that we shift to the offset video carrier by a right circular shift: $\{H_k'\} = \mathrm{FFT}_N\{h_n'\}$; $H_k'' = H_{k+N/2}'$, $k = 0, 1, \ldots, N/2 - 1$; $H_k'' = H_{k-N/2}'$, $k = N/2, \ldots, N - 1$. The coefficients H_k'' are now multiplied with the corresponding range-compression filter coefficients to produce a combined compression/interpolation filter.

To maintain the required α to $|\alpha| < 1$, after interpolation, compression, and basebanding, it is necessary to re-index the rows of the complex (compressed) data array. This implements the integer part of the required shifts. Thus, in Fig. 17, drawn for the case $f_{Dc}' < 0$, the bottom three rows are not shifted, the next three are shifted left by one cell, the next three are shifted by two cells, etc., through all rows. This shifting simply amounts to storing each range line appropriately at the output of the compression/interpolation filter.

Each row in general will be associated with a different value of α: $\alpha = [\Delta r]/\delta r$, where $[\Delta r]$ is the fractional part of Δr, the required range shift, and δr is the width of a complex range bin. To avoid the necessity of computing the interpolating filter coefficients during data compression, α is quantized into eight equal levels, and eight interpolating filters are separately combined with the range compression matched filter. The appropriate one of these eight filters is used according to the value of α.

After this process, the data corresponding to a point target at some arbitrary beam center slant range r_c lie within 1/8 of a complex range bin of the locus given by

$$\begin{aligned}\hat{r} &= r_c - (\lambda f_{Dc}/2)(\tau - \tau_c) - (\lambda K_{az}/4) \\ &\quad \times (\tau - \tau_c)^2 - \Delta r \\ &= r_c - (\lambda/2)(f_{Dc} - f_{Dc}')(\tau - \tau_c) \\ &\quad - (\lambda K_{az}/4)(\tau - \tau_c)^2 + \lambda f_{Dc}'\tau_c/2 .\end{aligned}$$

For Seasat, nominally $K_{az} = -510$ hertz per second and $\lambda = 0.235$ meter. Over the 100 kilometer swath, $|f_{Dc} - f_{Dc}'| \lesssim 200$ hertz, and for a point target, $|\tau - \tau_c| \lesssim 1.25$ seconds. Thus, the data migrate at most over approximately 60 meters (i.e., nine complex range bins) due to the mismatch of f_{Dc} and f_{Dc}', and at most approximately seven bins due to curvature. The term $\lambda f_{Dc}'\tau_c/2$ represents a skewing of the final image, which can be removed after azimuth compression.

The quadratic and residual linear range migration depend on τ_c. To remove this dependence, a fast Fourier transform is taken on each azimuth line of data to obtain a Doppler spectrum. Since the Doppler signal has a large time-bandwidth product,

$$\tau - \tau_c = (f - f_{Dc})/K_{az} ,$$

and the residual range migration correction needed is

$$\begin{aligned}\Delta' r &= -(\lambda/2)(f_{Dc} - f_{Dc}')(\tau - \tau_c) \\ &\quad - (\lambda K_{az}/4)(\tau - \tau_c)^2 \\ &= -(\lambda/2K_{az})(f_{Dc} - f_{Dc}')(f - f_{Dc}) \\ &\quad - (\lambda/4K_{az})(f - f_{Dc})^2 .\end{aligned}$$

For each value of r_c, the Doppler spectrum is assembled from data located at range $r_c + \Delta' r$ for each frequency, f. Interpolation is needed, since $\Delta' r$

is not usually an integral number of complex bins. Simple linear interpolation is used between the two range bins adjacent to $r_c + \Delta' r$. This finally corrects the last range migration term, and the spectrum is compressed with the appropriate azimuth filter.

The algorithm discussed above can be illustrated using the Goldstone image. Figure 18 shows the Goldstone target energy before and after re-indexing and interpolation to remove the nominal linear range walk. The curvature (quadratic) component is still evident. Figure 19 shows the Doppler spectra of the re-indexed data along columns (range bins) of memory. The two branches of the parabola, centered at two different azimuth times, τ_1 and τ_2, generate spectral content at frequencies $f_{D1} \approx K_{az}(\tau_1 - \tau_0)$ and $f_{D2} \approx K_{az}(\tau_2 - \tau_0)$. After quadratic range curvature correction, these spectra merge into a single Doppler spectrum (Fig. 20), corresponding to data along the parabolic trajectory in memory. The azimuth compression filter can then be applied, with the result seen in Fig. 21.

The azimuth filter parameters f_{Dc} and K_{az} needed for range walk correction and azimuth compression are determined off-line. If precise satellite position, velocity, and attitude (beam pointing) data were available, a calculation based on orbital mechanics could accurately determine slant range, $r(\tau)$, to any target point, as well as $\dot{r}(\tau)$ and $\ddot{r}(\tau)$, and hence f_{Dc} and K_{az}. However, these orbital and attitude data are often either not available or are not available with sufficient accuracy. It is necessary, therefore, to estimate f_{Dc} and K_{az} directly from the radar data.

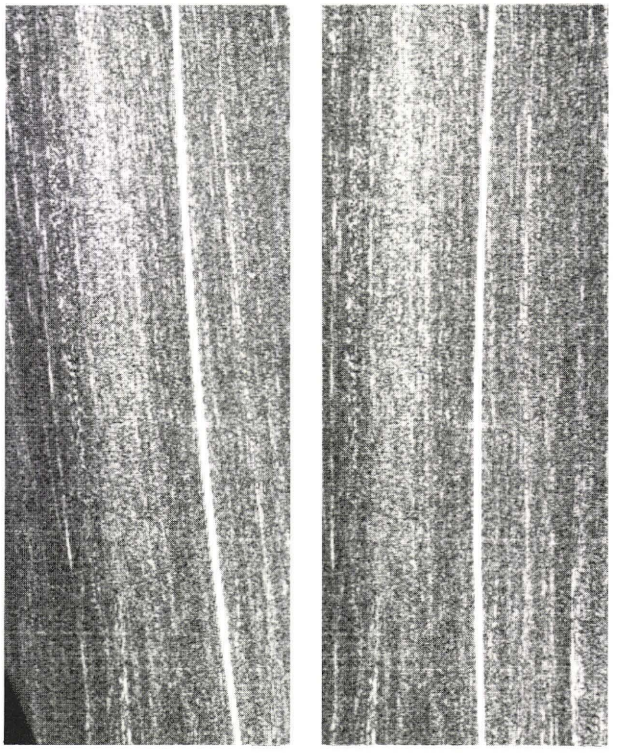

Figure 18—Range migration of Goldstone antenna before and after nominal correction.

From orbital mechanics, the expression for $r(\tau)$ can be found[6] in terms of the radar platform (satellite) position vector and attitude parameters and the coordinates of the image point on the earth's surface. For a nearly circular orbit, the filter parameters as functions of range are given (to a good approximation) by

$$f_{Dc} = a_1 + a_2 \sqrt{1 - (h/r_c)^2} \ ,$$

$$K_{az} = -2V^2/\lambda r_c \ ,$$

where h is satellite altitude, a_1 and a_2 are certain constants, and

$$V = V_s / \sqrt{1 + h/R_e} \ ,$$

where V_s is the satellite's speed in its orbit and R_e is the local earth radius.

Accepting these approximations, schemes can be derived for automatic measurement of f_{Dc} ("clutter-lock") and K_{az} ("autofocus"). Raw (uncompressed) offset video range data are converted to baseband by discarding the negative-frequency portion of the corresponding spectrum and down-shifting the result from the video offset frequency to baseband. The resulting

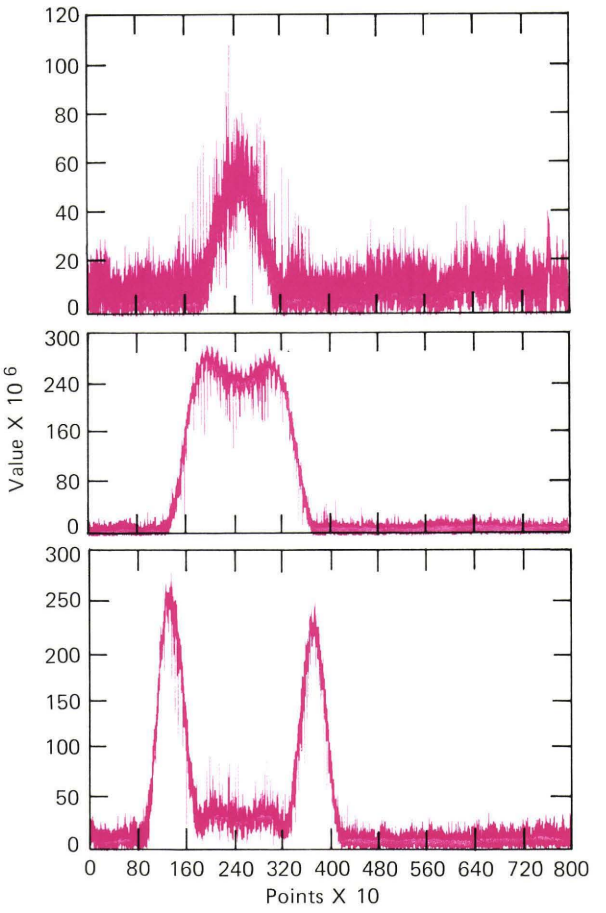

Figure 19—Doppler spectra for three range bins through and adjacent to Goldstone antenna showing the effect of range curvature on Goldstone data.

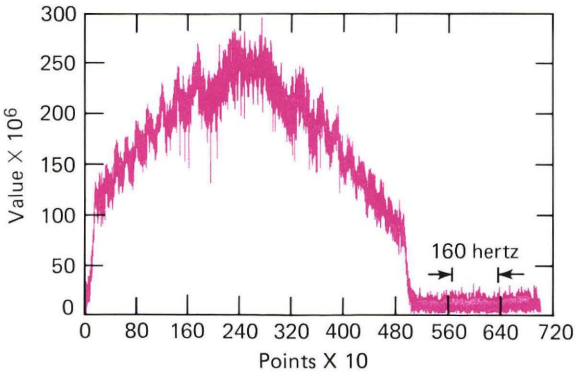

Figure 20—Spectrum of Goldstone data after correction for quadratic and residual linear components of range migration.

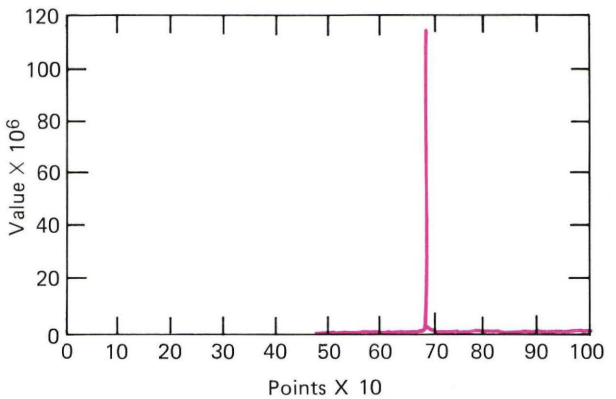

Figure 21—Goldstone target after azimuth compression of Doppler spectrum with complete (linear and quadratic) range migration correction.

complex data are used to form Doppler spectra by Fourier transformation in the azimuth direction for various constant slant ranges, without compensation for range migration. Specifically, some number of adjacent range bins are selected (e.g., 10) and the corresponding Doppler amplitude spectra are computed. These 10 spectra are averaged, and the average amplitude spectrum is correlated with the antenna pattern. The correlation peak is taken as an estimate of f_{Dc} at the mean r_c of the 10 bins averaged, using the assumption that the peak signal occurs at beam center. This procedure is repeated some number of times (e.g., 50) uniformly spaced across the swath, and the resulting f_{Dc} values are smoothed using the model above to determine the unknown constants. The resulting formula then yields f_{Dc} at any r_c of interest across the swath.

In the case of autofocus, some nominal value is chosen for the parameter β in the model $K_{az} = \beta/r_c$, and the full processing is carried out to produce an image in slant range and azimuth coordinates, over some two-dimensional region chosen small enough that β is sensibly constant in the corresponding data. The actual radar data will, however, correspond generally to some $\beta' \neq \beta$, so that the processed data will have azimuth compression filters mismatched by $\delta K = K - K' = (\beta - \beta')/r_c = (\delta\beta)/r_c$. We need to measure $\delta\beta$ and correct β.

Suppose then that an azimuth line of data is available for which the true azimuth chirp rate is K_{az}, and that these data are filtered with a mismatched compression filter having a chirp rate, K'_{az}. Then, for reasonable values of mismatch $\delta\beta$, and especially in the (usual) presence of weighting for sidelobe control, the envelope of the "matched" filter output still has a clear peak, but not at τ_0. The image registers, not at τ_0, but with a shift:

$$\delta\tau = f_{Dc}(1/K - 1/K') \approx (f_{Dc} r_c/\beta^2)\ \delta\beta\ .$$

This relation suggests a multi-look (sub-aperture) correlation procedure to measure $\delta\beta$. In a multi-look system, the same image can be produced in two different looks with two values of f_{Dc}, namely, the Doppler center frequencies of two of the looks, say f_{c1} and f_{c2}. Corresponding azimuth lines in the two images are displaced relative to each other by

$$\Delta = \delta\tau_1 - \delta\tau_2 = (f_{c1} - f_{c2})\, r_c \delta\beta/\beta^2\ .$$

Forming the cross-correlation function

$$\rho(x) = \sum_I \alpha(r_c,\ \tau + x r_c)\ \alpha(r_c,\ \tau)\ ,$$

where I is a region in the (r_c, τ) plane and $\alpha(r_c, \tau)$ is the image intensity, the function $\rho(x)$ can be expected to peak at $x = (f_{c1} - f_{c2})\delta\beta/\beta^2$, yielding a measurement of $\delta\beta$, which then determines K_{az}. From the models of $f_{Dc}(r_c)$ and $K_{az}(r_c)$ thus determined, the azimuth filter constants are available for any r_c of interest. In operation, the filters need to be updated only periodically, say once each 64 range bins across the swath.

CONCLUSION

The APL processor is still evolving. Nevertheless, the processor at this stage of development provides a reasonably flexible and efficient tool for investigating the SAR imaging process, and it is being routinely used as such.

REFERENCES

[1] D. E. Barrick and C. T. Swift, "The SEASAT Microwave Instruments in Historical Perspective," *IEEE J. Oceanic Eng.* **OE-5**, 74-79 (1980).
[2] R. L. Jordan, "The SEASAT-A Synthetic Aperture Radar System," *IEEE J. Oceanic Eng.* **OE-5**, 154-164 (1980).
[3] R. K. Moore, "Radar Sensing of the Ocean," *IEEE. J. Oceanic Eng.* **OE-10**, 84-113 (1985).
[4] C. E. Cook and M. Bernfeld, *Radar Signals, an Introduction to Theory and Application*, Chap. 6, Academic Press, New York (1967).
[5] A. Papoulis, *The Fourier Integral and Its Applications*, McGraw-Hill, New York (1962).
[6] B. C. Barber, *Theory of Digital Imaging from Orbital Synthetic Aperture Radar*, Technical Report 83 079, Royal Aircraft Establishment, Farnborough (1983).

ACKNOWLEDGMENTS—Many people have helped the authors during the development of the SAR processing capability we have described above. Funds were provided by the Defense Advanced Research Projects

Agency, with A. J. Bruckheim as project monitor. S. W. McCandless suggested the SAR problem as a candidate for application of the FPS-164 processor. H. Runge and W. Noack of the Deutsche Forschungs- und Versuchsanstalt für Luft- und Raumfahrt e.V. (German Aerospace Research Establishment), B. Barber of the Royal Aircraft Establishment (Great Britain), E.-A. Herland of the Norwegian Defence Research Establishment, and J. Curlander of the Jet Propulsion Laboratory provided valued technical discussions. T. D. Taylor of APL has been unfailingly encouraging at every stage of the effort. D. G. Tilley of APL has consistently provided high-quality image processing services. C. P. Mrazek of APL constructed important sections of the processor code, and G. D. Smith of APL contributed valuable support and discussion.

THE AUTHORS

ROBERT N. McDONOUGH (center) is a member of the Principal Professional Staff and is an engineer in APL's Submarine Technology Department. After receiving the B.E.S. (1956) and D. Eng. (1963) degrees in electrical engineering from The Johns Hopkins University, he was involved for four years in missile and sonar systems analysis at Bell Telephone Laboratories. He was a member of the electrical engineering faculty at the University of Delaware for 14 years and served as Assistant Dean of Engineering until joining APL in 1980. Dr. McDonough's current technical interest is signal and information processing, especially as applied to sonar and synthetic aperture radar systems. He is program coordinator of the part-time electrical engineering master's degree program at Johns Hopkins, an associate editor of the *IEEE Transactions on Acoustics, Speech, and Signal Processing,* and a Registered Professional Engineer in the state of Delaware.

BARRY E. RAFF (left) was born in Indianapolis in 1945. He received the B.S. degree from the Rose-Hulman Institute in 1967, the M.S. degree from Case Western Reserve University in 1969, and the Certificate of Continuing Engineering Studies from The Johns Hopkins University in 1972. He joined APL's Fleet Systems Department in 1968, where he did research on radar sea clutter and adaptive video processor design. He transferred to the Submarine Technology Department in 1975, where he investigated radar scatter from the ocean surface. Mr. Raff, a member of the Principal Professional Staff, is the assistant supervisor of the Information Processing Group and is conducting research and development in synthetic aperture radar processing techniques. He is a member of the IEEE.

JOYCE L. KERR (right) is a computer specialist in the Information Processing Group of the Submarine Technology Department. She received a B.A. from Cornell University and completed her graduate studies at Columbia University. After receiving a Ph.D. in experimental psychology in 1969, she pursued full-time research in neurophysiological responsiveness to acoustic stimuli at the University of Pittsburgh School of Medicine. In 1977, her experience in scientific computer applications took her to NASA's Goddard Space Flight Center, where she supervised software development for the Seasat and Solar Maximum Mission operations control centers on a Sperry Univac contract. Since joining APL in 1980, her interests have focused on digital signal processing and scientific applications for array processors.